Competition between fusion-fission and quasifission processes in the ^{32}S+^{182,184}W reactions

H. Q. Zhang,* C. L. Zhang, C. J. Lin, Z. H. Liu, and F. Yang

China Institute of Atomic Energy, P. O. Box 275, Beijing 102413, China

A. K. Nasirov†

Joint Institute for Nuclear Research, 141980 Dubna, Russia

G. Mandaglio, M. Manganaro, and G. Giardina

Dipartimento di Fisica dell' Università di Messina, 98166 Messina,

and Istituto Nazionale di Fisica Nucleare, Sezione di Catania, Italy

(Dated: Today)

Abstract

The angular distributions of fission fragments for the ^{32}S+^{184}W reaction at center-of-mass energies of 118.8, 123.1, 127.3, 131.5, 135.8, 141.1 and 144.4 MeV were measured. The experimental fission excitation function is obtained. The fragment angular anisotropy ($\mathcal{A}_{\rm exp}$) is found by extrapolating the each fission angular distributions. The measured fission cross sections of the ^{32}S+^{182,184}W reaction are decomposed into fusion-fission, quasifission and fast fission contributions by the dinuclear system model. The total evaporation residue excitation function for the ^{32}S+^{184}W reaction calculated in the framework of the advanced statistical model is in good agreement with the available experimental data up to about $E_{\rm c.m.} \approx 160$ MeV. The theoretical descriptions of the experimental capture excitation functions for both reactions and quantities K_0^2, $< \ell^2 >$ and $\mathcal{A}_{\rm exp}$ which characterize angular distributions of the fission products were performed by the same partial capture cross sections at the considered range of beam energy.

PACS numbers: 25.70.Jj, 25.70.Gh, 25.85.-w

*School of Physics, Peking University 100871 Beijing, China; Electronic address: huan@ciae.ac.cn

†Institute of Nuclear Physics, 100214, Tashkent, Uzbekistan; Electronic address: nasirov@jinr.ru

I. INTRODUCTION

Studies of fusion-fission reactions between heavy ion projectile and heavy target nuclei have demonstrated to be very useful in developing an understanding of the nuclear reaction dynamics. Especially with the development of radioactive nuclear beams and the superheavy element synthesis, this study is becoming a hot topic again. Very recently, the synthesis of the heaviest elements of 114, 115, 116 and 118 by using the hot-fusion reactions [1, 2] with actinide targets and of 112 and 113 by using the cold-fusion reactions [3, 4] with lead-based targets of shell closed spherical nuclei have been reported. The cross section of the evaporation residue (ER) formation being a superheavy element is very small: some picobarns, or even some percents of picobarn at synthesis of the element Z=113.

There are two main reasons causing a hindrance to the ER formation in the reactions with massive nuclei: the quasifission and fusion-fission processes. The ER formation process is often considered as third stage of the three-stage process. The first stage is a capture–formation of the dinuclear system (DNS) after full momentum transfer of the relative motion of colliding nuclei into the deformed shape, excitation energy and rotational energy. The capture takes place if the initial energy of projectile in the center-of-mass system is enough to overcome the interaction barrier (Coulomb barrier + rotational energy of the entrance channel). The study of dynamics of processes in heavy ion collisions at the near Coulomb barrier energies showed that complete fusion does not occurs immediately in the case of the massive nuclei collisions [5–8]. The quasifission process competes with formation of compound nucleus (CN). This process occurs when the DNS prefers to break up into fragments instead of to be transformed into fully equilibrated CN. The number of events going to quasifission increases drastically by increasing the sum of the Coulomb interaction and rotational energy in the entrance channel [9, 10]. Another reason decreasing yield of ER is the fission of a heated and rotating CN which is formed in competition with quasifission. The stability of massive CN decreases due to the decrease in the fission barrier by increasing its excitation energy $E^*_{\rm CN}$ and angular momentum L [11–13]. Because the stability of the transfermium nuclei are connected with the availability of shell correction in their binding energy [14, 15] which are sensitive to $E^*_{\rm CN}$ and values of the angular momentum. To find favorable reactions (projectile and target pair) and the optimal beam energy range leading to larger cross sections of synthesis of superheavy elements, we should establish conditions

to increase as possible the events of ER formation.

The total evaporation residue and fusion-fission excitation functions for the ^{32}S+^{182,184}W reactions are calculated in the framework of the advanced statistical model [11–13]. The results of calculation are in good agreement with the experimental data presented in Ref. [16] for the ^{32}S+^{184}W reaction up to $E_{\rm c.m.} \simeq 160$ MeV. The dip of the theoretical curve from experimental data at high excitation energies $E_{\rm c.m.} \simeq 160$ MeV is caused by the fact that statistical model can not reproduce the cross section of formation of reaction products by the nonequlibrium mechanism without formation of the compound nucleus in equlibrium state.

To determinate the ER cross section $\sigma_{\rm ER}(E)$ we used the partial fusion cross section as initial data about the heated and rotating CN with given excitation energy E and angular momentum ℓ [6]:

$$\sigma_{\rm ER}(E) = \sum_{l=0}^{\infty}(2l+1)\sigma_{\rm fus}^{(l)}(E)W_{\rm sur}(E,l). \tag{1}$$

The entrance channel effects can be studied [17] by analyzing the partial fusion cross section $\sigma_{\rm fus}^{l}(E)$ which is defined by the expression:

$$\sigma_{\rm fus}^{(l)}(E) = \sigma_{\rm capture}^{(l)}(E)P_{\rm CN}(E,l). \tag{2}$$

The theoretical cross section of capture includes the contributions of all fragment yields from full momentum transfer reactions:

$$\sigma_{\rm cap}(E_{\rm c.m.}) = \sigma_{\rm ER}(E_{\rm c.m.}) + \sigma_{\rm f}(E_{\rm c.m.}) + \sigma_{\rm qf}(E_{\rm c.m.}) + \sigma_{\rm fast\,fission}(E_{\rm c.m.}), \tag{3}$$

where $\sigma_{\rm ER}$, $\sigma_{\rm f}$, $\sigma_{\rm qf}$, and $\sigma_{\rm fast\,fission}$ are the evaporation residue, fusion-fission, quasifission and fast fission cross sections, respectively.

The pure cross section of the complete fusion must include only evaporation residues and fusion-fission cross sections

$$\sigma_{\rm fus}^{\rm (pure)} = \sigma_{\rm ER} + \sigma_{\rm ff}. \tag{4}$$

The experimental value of $\sigma_{\rm fus}$ reconstructed from the detected fissionlike fragments and evaporation residues:

$$\sigma_{\rm fus} = \sigma_{\rm ff} + \sigma_{\rm qf} + \sigma_{\rm fast\,fis} + \sigma_{\rm ER}, \tag{5}$$

where $\sigma_{\rm ff}$, $\sigma_{\rm qf}$, and $\sigma_{\rm fast\,fis}$ are the contributions of fusion-fission, quasifission and fast fission processes, respectively, and $\sigma_{\rm ER}$ is the ER contribution.

Thus, the estimations of $P_{\rm CN}$ and $W_{\rm sur}$ are the key point for the research of the fusion reaction products, especially for the synthesis of superheavy elements.

The presence of quasifission fragments in the measured yield of fissionlike fragments is determined by the large values of anisotropy in their angular distribution (see Refs.[5, 18, 19], and references therein) and by the increasing yield of fragments with masses near proton magic numbers 28, 50, 82 and neutron magic numbers 50, 82, 126 [20, 21]. But the mass and angular distributions of quasifission products can overlap with ones of fusion-fission products. The sizes of each overlap in the both mass and angular distributions depend on the beam energy and mass asymmetry of reacting nuclei. Therefore, quantitative estimations of contributions of quasifission and fusion-fission fragments in the measured fissionlike fragments is a nontrivial task up to now. This means that the estimation of the pure fusion cross section from the measured data of fission fragments and evaporation residues is still an ambiguous task.

In this paper we have analyzed the angular distribution of fission fragments and fission excitation function of the ^{32}S+^{184}W reaction measured at the center-of-mass energies of 118.8, 123.1, 127.3, 131.5, 135.8, 141.1 and 144.4 MeV in this work and similar data obtained from Ref. [22] at more large energies $E_{\rm c.m.}$ = 141.2–221.1 MeV. The angular anisotropy $\mathcal{A}_{\rm exp}$ of fission fragments measured in this work was found by extrapolating the each fission angular distributions to angles 0° and 90° by the method used in Ref. [23]. Then, the mean square angular momentum $\langle L^2 \rangle$ values were obtained. Hereafter we use for simplicity ℓ from the definition $L = \ell\hbar$.

The experimental data of the quantities K_0^2 and anisotropy of the angular distribution of the fission products of the ^{32}S+^{182}W [22] and ^{32}S+^{184}W (this work) reactions are described using angular momentum distribution of DNS calculated as a function of the orientation angle of symmetry axis of ^{182}W and ^{184}W.

We assumed the calculated capture cross sections to be equal to the experimental data of fissionlike fragments in order to decompose the measured fission cross section into fusion-fission, quasifission and fast fission contributions by the DNS model [6, 7, 10, 17]. We remind the difference between quasifission and fast fission. The quasifission is a break of the DNS into two fragments bypassing the stage of the CN formation. The fast fission process is the inevitable decay of the fast rotating mononucleus into two fragments without reaching the equilibrium compact shape of CN. Such mononucleus is formed from the DNS survived

against quasifission. At large values of the angular momentum $\ell > \ell_f$, where ℓ_f is a value of ℓ at which the fission barrier of the corresponding CN disappears, mononucleus immediately decays into two fragments [24]. As distinct from fast fission, the quasifission can occur at all values of ℓ at which capture occurs.

The present article is organized in the following way. The experimental procedure is presented in Section II. The experimental results of the fission fragment angular distributions and their anisotropy $A_{\rm exp}$, fission excitation function, mean square value $\langle l^2 \rangle$ of angular momentum and variance K_0^2 of the K distribution are presented in Section III. The comparison between the experimental data and theoretical results is discussed in Section IV. Finally, Section V is devoted to the conclusion of this work.

II. EXPERIMENTAL PROCEDURE

The experiment was performed at HI-13 tandem accelerator at China Institute of Atomic Energy, Beijing. A collimated ^{32}S beam with incident energies $E_{\rm lab}$ = 140, 145, 150, 155, 160, 165 and 170 MeV bombarded on a target of ^{184}W which was mounted at center of the scattering chamber. The ^{184}W target with thickness about 200 μg/cm^2 was evaporated on an about 20 μg/cm^2 carbon foil backing. Typical ^{32}S beam current range was 800-1000 enA monitored by a shielded suppressed Faraday cup at periphery of the chamber, because of the variety according to the bombarding energy and scattering angle. The beam energy loss in traveling half the target were calculated and was about 0.5 MeV.

The schematic view of the experimental set up is shown in Fig. 1. At the forward angles, an array of five Si detectors with depletion depth ranging from 200 to 300 μm, which covered the angular range of θ_L=14°-35°, 35°-55° and 55°-75° were mounted on the movable arm in the chamber and five masks were placed in the front of each detector for assuring the angular resolution. The detectors to the target distance was 27 cm. The Rutherford scattering was monitored at forward angle of θ_L=15° by four Si(Au) surface barrier detectors for the normalization of the cross section measurements.

In addition to these individual Si detectors, two groups of Si strip detectors were mounted on opposite sides of the beam. These Si strip detectors were 48×50 mm^2 in area and each detector consisted of 24 strips. Due to a lack of readout electronics, the strips were tied together in groups of eight for readout. Data from these strip detectors were recorded

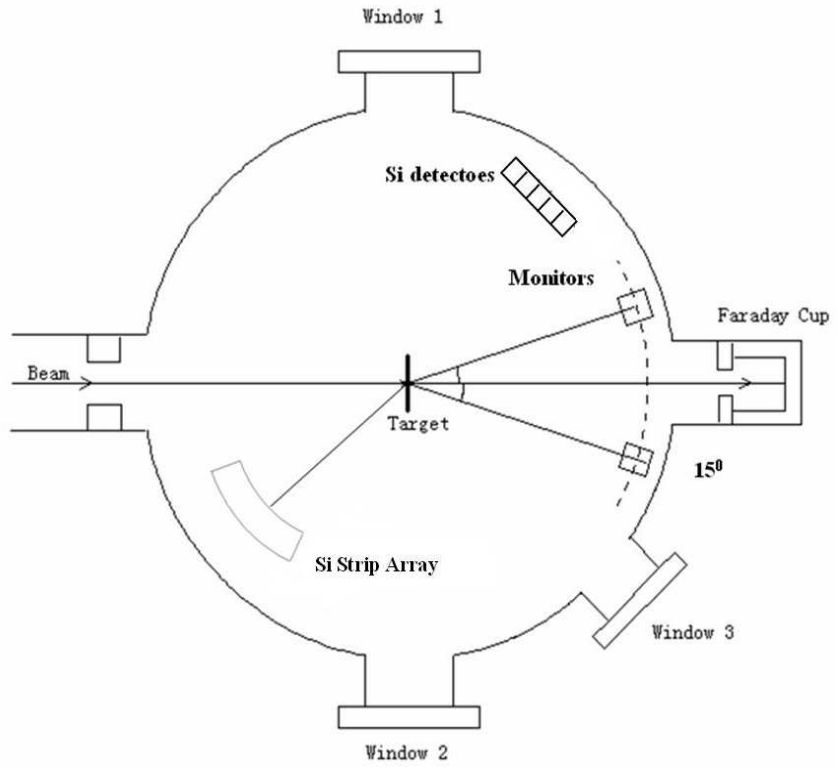

FIG. 1: Scheme of the experimental setup for the measurements of fission fragment angular distribution of binary reaction products. See explanations in the text for details.

in the coincidence mode with the requirement that each detector was struck by a fission fragment and the folding angle between the hits corresponded to a full momentum transfer event. To calculate the kinematics it was assumed all observed processes can be treated as binary reactions. This assumption was tested by examining the folding angle distribution of coincident fragments in the Si detector and the Si strip detectors. The average folding angle agrees with the expectations based on total fission kinetic energies taken from the Viola systematics [25].

To obtain the absolute cross sections, we measured the solid angle by using the α-particles from the ^{241}Am source and the elastic scattering products. Centering of the beam on the target was ensured by the four monitor detectors. A gate was set on the fission event and data were collected by the coincident mode.

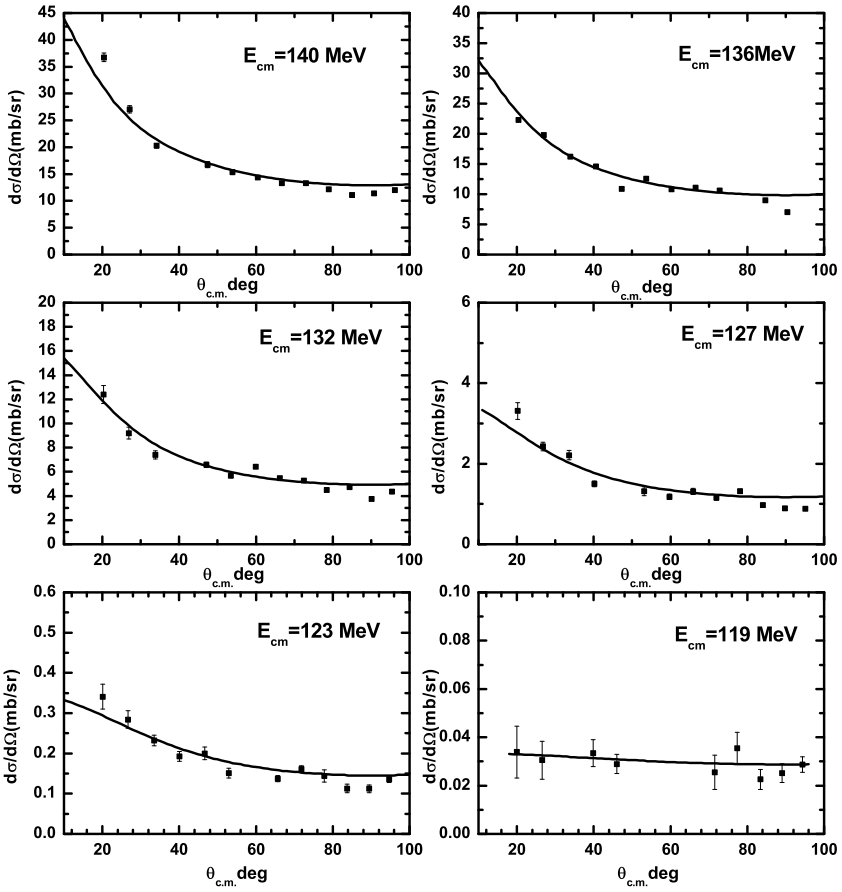

FIG. 2: Fission fragment angular distributions for the ^{32}S+^{184}W reaction. Incident energies are shown in the figure. The experimental data are shown with the fitting curve, which is used to determine the anisotropy $A_{\rm exp}$ of the fragment angular distribution and mean square values of angular momentum from these events.

III. EXPERIMENTAL RESULTS

A. Fission fragment angular distributions

The fission fragment angular distributions were measured using the coincident detectors and are shown in Fig. 2. In fitting the angular distribution of the fission fragments we used the familiar expression as in Ref. [23]:

$$W(\theta) = \sum_{J=0}^{J_{\rm max}} \frac{(2J+1)^2 \exp[-(J+\frac{1}{2})^2 \sin^2\theta/4K_0^2] J_0[i(J+\frac{1}{2})^2 \sin^2\theta/4K_0^2]}{{\rm erf}[(J+\frac{1}{2})/(2K_0^2)^{1/2}]} \qquad (6)$$

assuming M=0, *i.e.* assuming the spins of the target and projectile were zero, where J_0 is the zero order Bessel function with imaginary argument and error function erf(x) is defined

TABLE I: The measured capture cross sections and the deduced values of $\mathcal{A}_{\rm exp}$ and K_0^2 for the ^{32}S+^{184}W reaction. The $E_{\rm c.m.}$ are the energies calculated as corresponding to the beam energies in the center of the target.

$E_{\rm c.m.}$ (MeV)	$E^*_{\rm CN}$ (MeV)	$\sigma_{\rm capture}$ (mb)	$\mathcal{A}_{\rm exp}$	K_0^2
118.8	37.2	0.04	1.51	114.71
123.1	41.5	2.35	2.16	124.35
127.3	45.8	22.97	2.27	132.09
131.5	50.0	81.01	2.74	140.01
135.8	54.3	132.27	3.06	148.67
141.1	58.5	189.33	3.28	157.35
144.4	61.8	237.06	3.80	155.09

as

$$\mathrm{erf}(x) = (2/\pi^{1/2}) \int_0^x \exp(-t^2) dt. \tag{7}$$

The measured values of $\sigma_{\rm capture}$ and the deduced values of $\mathcal{A}_{\rm exp}$ and K_0^2 for the ^{32}S+^{184}W reaction are presented in Table I. $J_{\rm max}$ is obtained by reproducing the capture cross section. The K_0^2 value is found by fitting the angular distribution at known $J_{\rm max}$ from the total fission cross section. It is seen from Fig. 2 that the anisotropy of angular distribution increases by increasing collision energy $E_{\rm c.m.}$.

B. Capture cross section

In order to deduce the capture cross section from the data, the Si strip detectors operating in the coincidence mode were used. Each fission event was selected on the basis of the correct value of energy and of the folding angle corresponding to complete momentum transfer using the forward Si detectors as a "trigger" detector. After correction for the efficiency of the Si strip detectors, a differential cross section $d\sigma/d\Omega(\theta)$ was obtained. The total cross section was deduced from the integration of the differential cross sections.

The resulting experimental values of the capture cross sections are shown in Table I and Fig. 5 where they are compared with the theoretical results. Due to the small cross section of ER in the reaction under consideration [16], the total measured fission cross section is assumed to be equal to the theoretical capture cross section and it was decomposed into fusion-fission, quasifission and fast fission parts in the framework of the DNS model mentioned in Section I. The comparison of the measured capture cross section, anisotropy, mean square values of angular momentum, and variance K_0^2 with the corresponding experimental data is discussed in Section IV.

C. Anisotropy of fission-fragments and mean square angular momentum values

The experimental values of the anisotropy $\mathcal{A}_{\rm exp}$ are found by extrapolating the fission angular distributions to angles 0° and 90° by the method used in Ref. [23]. The anisotropies as a function of center-of-mass energies are shown in Table I and Fig. 11 where they are compared with the theoretical results. Using the approximate relation between the anisotropy and the mean square angular momentum (see Section IV for details), the mean square angular momentum values $\langle l^2 \rangle$ are deduced from the experimental anisotropies and shown in Fig. 12.

IV. THEORETICAL DESCRIPTION AND COMPARISON WITH MEASURED DATA

The experimental data for the excitation function of fissionlike products in the ^{32}S+^{184}W reaction were analyzed in the framework of the DNS model [9, 10, 17, 26, 27]. The capture, fusion, quasifission, fusion-fission, evaporation residue, and fast fission excitation functions have been calculated for this reaction. According to the DNS model a capture event is the trapping of the collision path into the potential well (see Fig. 3) after dissipation of the sufficient part of the relative kinetic energy of a projectile nucleus in the center-of-mass coordinate system. At capture the full momentum transfer from the relative motion of nuclei into excitation energy of dinuclear system takes place. Certainly the presence of a potential pocket and adequacy of the collision energy $E_{\rm c.m.}$ to overcome the interaction barrier of the entrance channel $V_{\rm B}$ are necessary conditions to occur capture as shown in Fig. 3. Thus

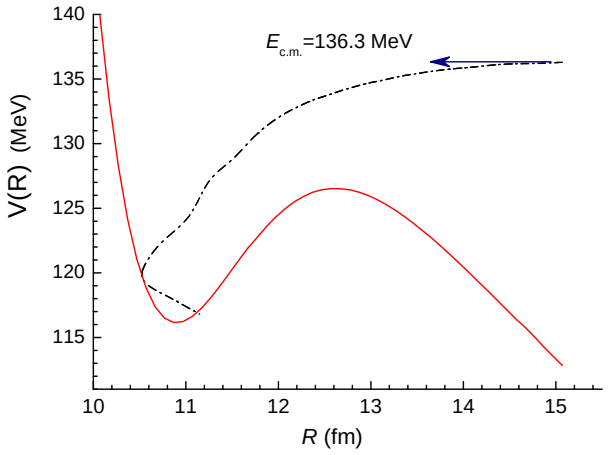

FIG. 3: (Color online) Illustration of capture path (dot dashed line) into potential well (solid line) as the numerical solution of the equation of relative motion of colliding nuclei with the initial energy $E_{\rm c.m.} = 136.3$ MeV and L=0 for the ^{32}S+^{184}W reaction.

capture leads to forming DNS which characterized by mass (charge) asymmetry of its nuclei, rotational energy $V_{\rm rot}$ and excitation energy $E^*_{\rm DNS}$. The relative energy of nuclei is relaxed, therefore, the total kinetic energy of fragments formed at its decay are close to the Viola systematics [25].

The nucleus-nucleus potential $V(Z, A, R)$ is a sum of the Coulomb $V_{\rm C}(Z, A, R)$ and nuclear interaction $V_{\rm N}(Z, A, R)$, as well as the rotational energy $V_{\rm rot}(Z, A, R, \ell)$:

$$V(Z, A, R, \ell) = V_{\rm C}(Z, A, R) + V_{\rm N}(Z, A, R) + V_{\rm rot}(Z, A, R, \ell) \tag{8}$$

where $Z = Z_1$ and $A = A_1$ are the charge and mass numbers of one of fragments forming the DNS, respectively, while the charge and mass numbers of another fragment are equal to $Z_2 = Z_{\rm CN} - Z$ and $A_2 = A_{\rm CN} - A$, respectively, where $Z_{\rm CN}$ and $A_{\rm CN}$ the charge and mass numbers of being formed CN; R is the relative distance between the centers of nuclei forming DNS. The partial capture cross section is found by solution of kinetic equation for the relative motion and orbital angular momentum ℓ for the different orientation angle $\alpha_{\rm T}$ of the target nucleus as it was performed in Refs. [9, 17]. The fusion cross section is calculated from the branching ratio $P_{\rm CN}(Z)$ of the decay rates of overflowing the border of the potential well ($B^{(Z)}_{\rm qf}$) along R at a given mass asymmetry (decay of DNS–quasifission) over the barriers on mass asymmetry axis $B^*_{\rm fus}$ for the complete fusion or $B^{(Z)}_{\rm sym}$ in opposite direction to the symmetric configuration of DNS (see Fig. 4):

$$P^{(Z)}_{\rm CN}(E^*_{\rm DNS}) \approx \frac{\Gamma^{(Z)}_{\rm fus}(B^*_{\rm fus}, E^*_{\rm DNS})}{\Gamma^{(Z)}_{\rm (qf)}(B_{\rm qf}, E^*_{\rm DNS}) + \Gamma^{(Z)}_{\rm (fus)}(B^*_{\rm fus}, E^*_{\rm DNS}) + \Gamma^{(Z)}_{\rm sym}(B_{\rm sym}, E^*_{\rm DNS})}, \tag{9}$$

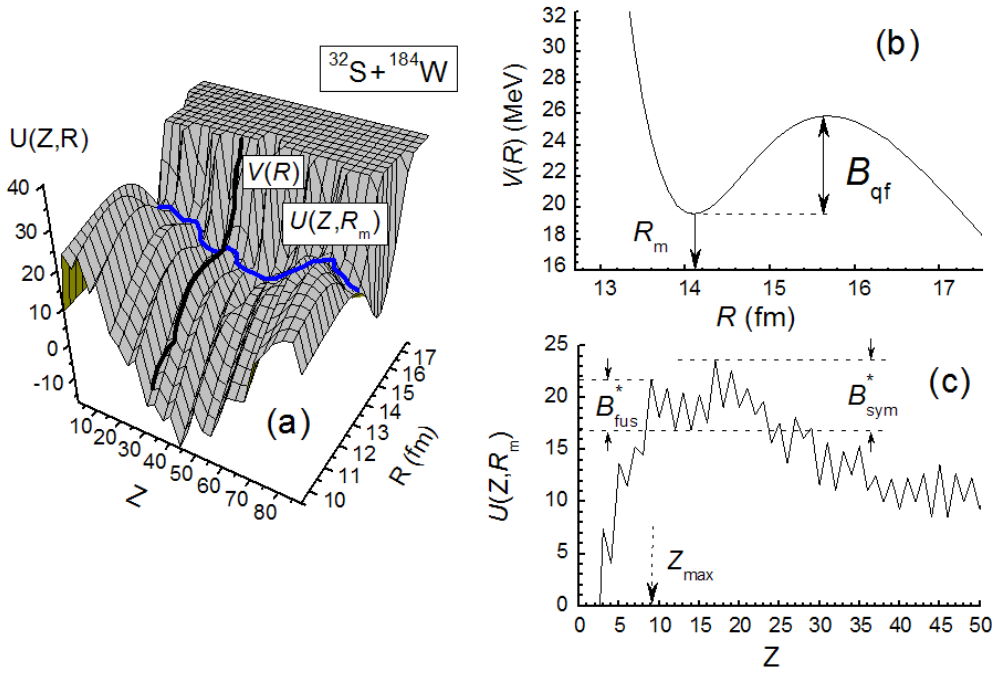

FIG. 4: (Color online) The potential energy surface for a dinuclear system leading to the formation of the ^{216}Th* CN as a function of the relative distance R between centers of interacting nuclei and their charge numbers Z, panel (a); the nucleus-nucleus interaction potential $V(R)$ shifted on the Q_{gg}-value for the ^{32}S + ^{184}W reaction, panel (b); the driving potential, $U_{\rm dr}(Z, R_m)$, which is a curve linking minimums corresponding to each charge asymmetry in the valley of the potential energy surface as a function of Z, panel (c).

where $\Gamma_{\rm fus}$, $\Gamma_{\rm qf}$ and $\Gamma_{\rm sym}$ are corresponding widths determined by the level densities on the barriers $B^*_{\rm fus}$, $B_{\rm qf}$ and $B^*_{\rm sym}$ involved in the calculation of $P_{\rm CN}$ are used in the model [8, 10, 17] based on the DNS concept [28]. Here $E^*_{\rm DNS}(Z_{\rm P}, A_{\rm P}, \ell) = E_{\rm c.m.} - V(Z_{\rm P}, A_{\rm P}, \ell, R_{\rm m})$ is the excitation energy of DNS in the entrance channel, where $Z_{\rm P}$ and $A_{\rm P}$ are charge and mass numbers of the projectile nucleus. $V(Z, A, R_{\rm m}, \ell)$ is the minimum value of the nucleus-nucleus potential well (for the DNS with charge asymmetry Z) and its position on the relative distance between the centers of nuclei is marked as $R = R_{\rm m}$ in Fig. 4b. The value of $B_{\rm qf}$ for the decay of DNS with the given charge asymmetry of fragments is equal to the depth of the potential well in the nuclear-nuclear interaction (see Fig. 4b). The intrinsic fusion barrier $B^*_{\rm fus}$ is connected with mass (charge) asymmetry degree of freedom of the DNS

and it is determined from the potential energy surface (Fig. 4a):

$$U(Z;R,\ell) = U(Z,\ell,\beta_1,\alpha_1;\beta_2,\alpha_2) = B_1 + B_2 + V(Z,\ell,\beta_1,\alpha_1;\beta_2,\alpha_2;R) - (B_{\rm CN} + V_{\rm CN}(\ell)). \tag{10}$$

Here, B_1, B_2 and $B_{\rm CN}$ are the binding energies of the nuclei in DNS and the CN, respectively, which were obtained from [29]; the fragment deformation parameters β_i are taken from the tables in [29–31] and α_i are the orientation angles of the reacting nuclei relative to the beam direction; $V_{\rm CN}(\ell)$ is the rotational energy of the CN. The distribution of neutrons between two fragments for the given proton numbers Z and Z_2 or ratios A/Z and A_2/Z_2 for both fragments were determined by minimizing the potential $U(Z;R)$ as a function of A for each Z.

The driving potential $U_{\rm dr}(Z) \equiv U(Z,R_{\rm m})$ is a curve linking minimums corresponding to each charge asymmetry Z in the valley of the potential energy surface from $Z = 0$ up to $Z = Z_{\rm CN}$ (see Fig. 4a and 4c). We define the intrinsic fusion barrier for the DNS with charge asymmetry Z as $B^*_{\rm fus}(Z,\ell) = U(Z_{\rm max}, R_{\rm m}(Z_{\rm max}),\ell) - U(Z,R_{\rm m}(Z),\ell)$, where $U(Z_{\rm max},\ell)$ is a maximum value of potential energy at $Z = Z_{\rm max}$ in the valley along the way of complete fusion from the given Z configuration. The $B^*_{\rm sym}(Z,\ell)$ is defined by the similar way as shown in Fig. 4c [17, 32].

The masses and charges of the projectile and target nuclei are not constant during capture and after formation of the DNS. The intense proton and neutron exchange between constituents of DNS is taken into account by calculation of the complete fusion probability $P_{\rm CN}$ as fusion from all populated DNS configurations according to the formula

$$P_{\rm CN}(E^*_{\rm DNS}(Z,A,\ell);\{\alpha_i\}) = \sum_{Z_{\rm sym}}^{Z_{\rm max}} Y_Z(E^*_{\rm DNS}(Z,A,\ell)) P^{(Z)}_{\rm CN}(E^*_{\rm DNS}(Z,A,\ell);\{\alpha_i\}) \tag{11}$$

where $E^*_{\rm DNS}(Z,A,\ell) = E^*_{\rm DNS}(Z_{\rm P},A_{\rm P},\ell) + \Delta Q_{\rm gg}(Z)$ is the excitation energy of DNS with angular momentum ℓ for a given value of its charge-asymmetry configuration Z and $Z_{\rm CN} - Z$; $Z_{\rm sym} = (Z_1 + Z_2)/2$; $\Delta Q_{\rm gg}(Z)$ is the change of $Q_{\rm gg}$-value by changing the charge (mass) asymmetry of DNS; $Y_Z(E^{*(Z)}_{\rm DNS})$ is the probability of population of the (Z, $Z_{\rm CN}$-Z) configuration at $E^{*(Z)}_{\rm DNS}$ and given orientation angles (α_1,α_2). It was obtained by solving the master equation for the evolution of the dinuclear system charge asymmetry (for details see Refs. [17, 18]).

The calculations were performed for the energy range $E_{\rm c.m.}$=119.5–220.5 MeV and initial values of the orbital angular momentum ℓ =0–150$\hbar$. Due to the deformed shape of

^{184}W ($\beta_2 = 0.24$ and $\beta_4 = -0.095$) in the ground state we included in our calculations a dependence of the excitation function of capture, complete fusion and quasifission on the orientation angle $\alpha_{\rm T}$ of its axial symmetry axis. The ground state shape of ^{32}S is spherical but the quadrupole (2^+) and octupole (3^-) collective excitations in spherical nuclei are taken into account as amplitudes of the zero-point motion mode of surface vibration by the same way as in Ref. [27]. The deformation parameters of the first excited quadrupole state $\beta_2^{(2+)} = 0.312$ (taken from Ref. [30]) and the ones of the first excited octupole state $\beta_3^{(3-)}$=0.41 (taken from Ref. [31]). The final results of the capture and complete fusion are obtained by averaging the contributions calculated for the different orientation angles ($\alpha_{\rm T}$=0°, 15°, 30°, ..., 90°) of the symmetry axis of the target nucleus:

$$\langle \sigma_{\rm fus}(E_{\rm c.m.}, l) \rangle = \int_0^{\pi/2} \sin\alpha_{\rm T} \sigma_{\rm fus}(E_{\rm c.m.}, l; \alpha_{\rm T}) d\alpha_{\rm T}. \quad (12)$$

These methods were developed and used in the Refs. [17, 26, 27]. The partial cross sections of CN formation at the given energy $E_{\rm c.m.}$ are used to calculate the ER formation and fusion-fission cross sections by the advanced statistical model [11–13]. The code takes into account the competition between evaporation of light particles (n, p, α, and γ) and fission processes along each step of the deexcitation cascade of CN. The effective fission barrier for CN and intermediate excited nuclei along the cascade are obtained taking into account the macroscopic fission barrier, predicted by the rotating droplet model as parameterized by Sierk [33], together with the microscopic corrections allowing for the angular momentum and temperature fade-out of shell corrections [29] to the fission barrier (see Refs. [7, 32, 34], and reference therein). The cross section of ER formed at each step x of the deexcitation cascade after the emission of $\nu(x)$n+$y(x)$p+$k(x)\alpha$+$s(x)\gamma$ particles (ν, y, k, s are numbers of neutrons, protons, α-particles and γ-quanta) from the hot CN is calculated by the formula[7, 10, 32]:

$$\sigma_{\rm ER}(E_x^*) = \sum_{Z_{l=0}}^{l_d} \sigma_{(x-1)}^l(E_x^*) W_{{\rm sur}(x-1)}(E_x^*, l), \quad (13)$$

where $\sigma_{(x-1)}^l(E_x^*)$ is the partial cross section of the intermediate nucleus formation at the $(x-1)$th step and $W_{{\rm sur}(x-1)}(E_x^*, \ell)$ is the survival probability of the $(x-1)$th intermediate nucleus against fission along the deexcitation cascade of CN; E_x^* is an excitation energy of the nucleus formed at the xth step of the deexcitation cascade. It is clear that $\sigma_{(0)}^l(E_0^*) = \sigma_{\rm fus}^l(E^*)$ at $E_{\rm CN}^* = E_0^* = E_{\rm c.m.} + Q_{\rm gg}$, where $Q_{\rm gg}$ is energy balance of reaction. The numbers

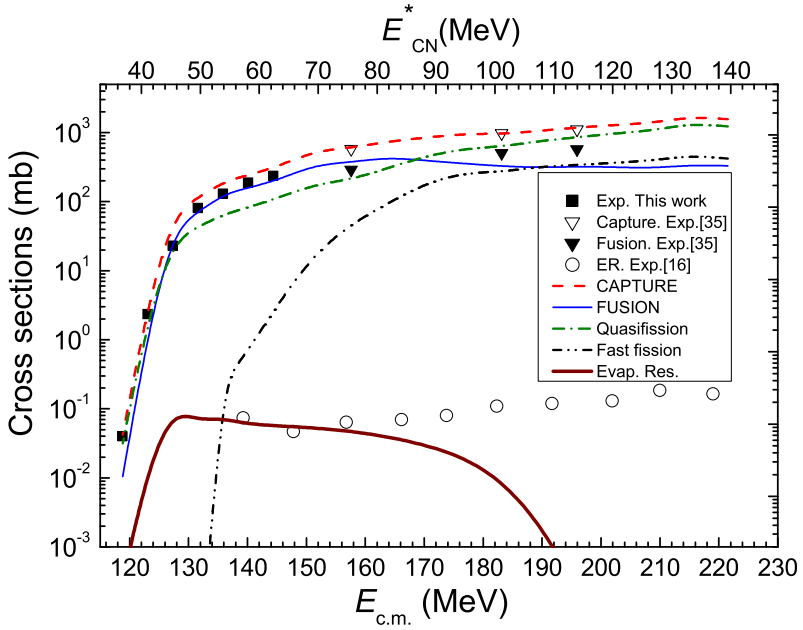

FIG. 5: (Color online) Experimental excitation functions of capture obtained in this work (squares) and in Ref. [35] (open down triangles), of fusion obtained in Ref. [35] (solid down triangles), of evaporation residues after emission of neutrons, protons and α-particles from ^{216}Th* compound nucleus for the ^{32}S+^{184}W reaction [16] (open circles) are compared with theoretical results by the DNS model for the capture (dashed line), complete fusion (thin solid line), quasifission (dot-dashed line), fast fission (dot-dot-dashed line) and total evaporation residues (thick solid line). Theoretical values of fusion-fission and fusion cross sections are nearly equal because the total cross section for the evaporation residues after emission of neutrons, protons and α-particles from ^{216}Th* compound nucleus are very small.

of the being emitted neutrons, protons, α-particles, γ-quanta, $\nu(x)$n, $y(x)$p, $k(x)\alpha$, and $s(x)\gamma$, respectively, are functions of the step x. The emission branching ratio of these particles depends on the excitation energy and angular momentum of the being cooled intermediate nucleus $A = A_{\rm CN} - (\nu(x) + y(x) + 4k(x))$ and $Z = Z_{\rm CN} - (y(x) + 2k(x))$ [7]. The results of calculation of the excitation functions for the ^{32}S+^{184}W and ^{32}S+^{182}W reactions are presented in Figs. 5 and 6, respectively, and they are compared with the available experimental data. In Fig. 5, the excitation functions of capture obtained in this work (squares) and in Ref. [35] (open down triangles), of complete fusion obtained in Ref. [35] (solid down triangles), of evaporation residues after emission of neutrons, protons and α-particles from ^{216}Th* compound nucleus for the ^{32}S+^{184}W reaction [16] (solid circles)

with theoretical results by the DNS model for the capture (dashed line), complete fusion (thin solid line), quasifission (dot-dashed line), fast fission (dot-dot-dashed line) and total evaporation residues (thick solid line). Theoretical values of fusion-fission and fusion cross sections are nearly equal because the total cross section for the evaporation residues after emission of neutrons, protons and α-particles from ^{216}Th* compound nucleus are small. The agreement between the experimental and theoretical capture cross sections was reached by changing the radius parameter C_R entered to rescale the nuclear radius:

$$R_1 = C_R\sqrt{(R_{\rm p}^2\, Z_1 + R_{\rm n}^2\,(A_1 - Z_1))/A_1}\,, \tag{14}$$

where $R_{\rm p}$ and $R_{\rm n}$ are the proton and neutron radii, respectively, obtained from Ref. [36]:

$$R_{\rm p} \;=\; 1.237(1 - 0.157(A-2Z)/A - 0.646/A)A^{1/3}, \tag{15}$$

$$R_{\rm n} \;=\; 1.176(1 + 0.25(A-2Z)/A + 2.806/A)A^{1/3}. \tag{16}$$

The presented results are obtained at $C_R = 0.925$ for all values of $E_{\rm c.m.}$. Using Eq.(12) we calculated the partial fusion cross sections which were used to estimate the cross sections of ER and fusion-fission by the advanced statistical model [11, 12]. Taking into account the dependence of the fission barrier ($B_{\rm f}$) of the rotating CN on its angular momentum we found a value of ℓ at which $B_{\rm f}$ disappears using the rotating finite range model by A. J. Sierk [33]: $\ell_{\rm B}$=68 for ^{214}Th and $\ell_{\rm B}$=70 for ^{216}Th. Then we calculate the fast fission contribution for $\ell > \ell_{\rm B}$

$$\sigma_{\rm fast\,fission}(E_{\rm c.m.}) = \sum_{\ell=\ell_{\rm B}}^{\ell=\ell_{\rm max}} (2\ell+1)\sigma_{\rm fus}(E_{\rm c.m.},\ell) \tag{17}$$

where $\ell_{\rm max}$ is the maximum value of angular momentum of the DNS for the given value of $E_{\rm c.m.}$. The value of $\ell_{\rm max}$ is found by solving the equations of motion for the radial distance and orbital angular momentum with the given values of $E_{\rm c.m.}$, ℓ_0 and $R_{\rm max} = 20$ fm.

In Fig. 5, the ER cross sections obtained by the advanced statistical model (see Refs. [11–13], and references therein) describing the full deexcitation cascade of the ^{216}Th* CN formed in the ^{32}S+^{184}W reaction are compared with the corresponding experimental data from Ref. [16]. The theoretical excitation function (thick solid curve) of the total evaporation residues is close to the measured data [16] up to $E_{\rm c.m.} \approx 160$. The dip of the theoretical curve at collision energies $E_{\rm c.m.} > 160$ MeV can be explained by production of the observed fragments in the nonequlibrium mechanism without formation of the compound nucleus in

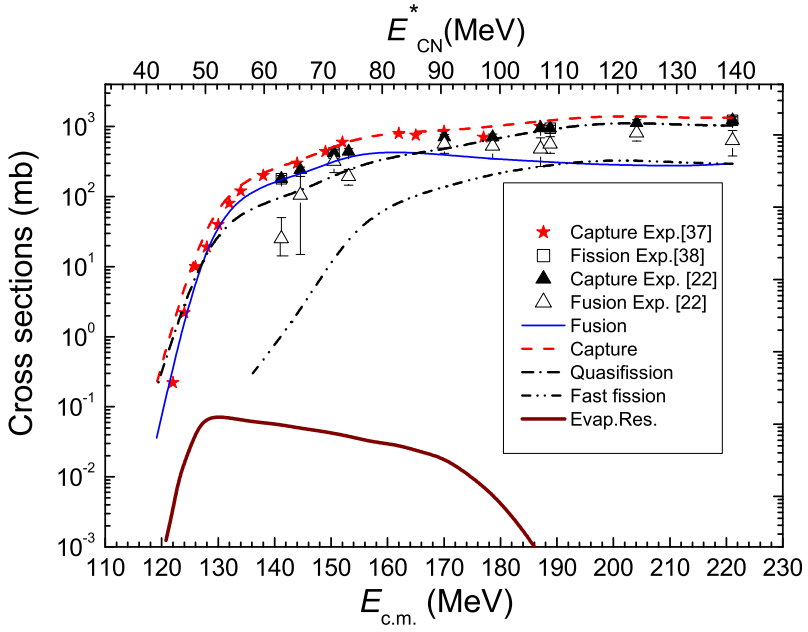

FIG. 6: (Color online) Comparison of the experimental excitation functions of fission (capture) obtained from Refs. [37] (stars), [22] (solid up triangles) and [38] (open squares) and of fusion obtained from Ref. [22] (open up triangles)) for the ^{32}S+^{182}W reaction with theoretical results by the DNS model for the capture (dashed line), complete fusion (thin solid line), quasifission (dot-dashed line), fast fission (dot-dot-dashed line). Theoretical values of fusion-fission and fusion cross sections are nearly equal because the calculated results of the total cross section for the evaporation residues after emission of neutrons, protons and α-particles from ^{214}Th* compound nucleus are small (thick solid line).

the statistical equlibrium state. The measured data in Ref. [16] could include the evaporation residues which are formed at incomplete fusion or multinucleon transfer reactions at $E_{\rm c.m.} > 160$ MeV. Because the number of evaporation residues formed from the heated and rotating CN should not increase at decreasing the complete fusion cross section by the increase in collision energy $E_{\rm c.m.}$. The hindrance to complete fusion at large beam energies is connected by the dependence of the quasifission and intrinsic fusion barriers of DNS on its angular momentum. The decrease in complete fusion probability at large collision energies is connected with the increase in the quasifission and fast fission events which are presented in Figs. 5 and 6. The ambiguity of the determination of complete fusion cross section from the measured yield of fissionlike products casts doubt on the reconstruction of complete fusion mechanism. Therefore, in the next Section, we will discuss the mechanisms causing

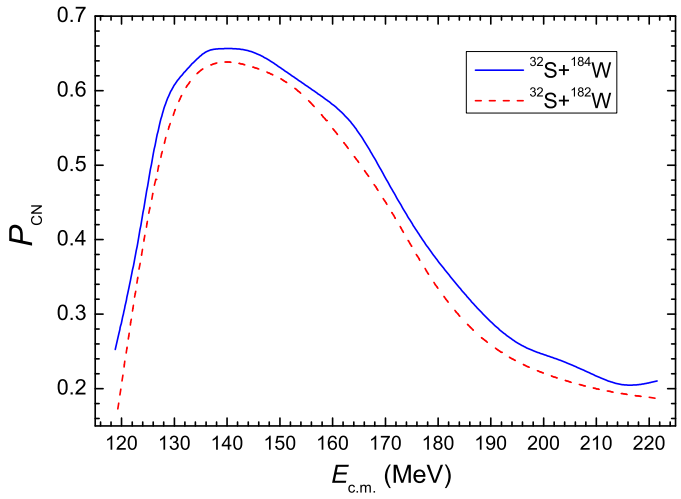

FIG. 7: (Color online) Theoretical values of the fusion probability $P_{\rm CN}$ for the ^{32}S+^{182}W (dashed line) and ^{32}S+^{184}W (solid line) reactions as a function of collision energy $E_{\rm c.m.}$.

hindrance to complete fusion.

A. Two regions of strong hindrance to complete fusion

The experimental fission excitation function is decomposed into contributions of fusion-fission, quasifission, and fast fission. The intense of hindrance to complete fusion is estimated by the fusion factor $P_{\rm CN}$ which was entered in Eq. (2) and it is determined by Eqs. (9) and (11). In Fig. 7 the calculated values of $P_{\rm CN}$ as a function of the beam energy for the ^{32}S+^{182}W (dashed line) and ^{32}S+^{184}W (solid line) reactions are presented. It is seen the hindrance to fusion is strong at very small and large values of the collision energy $E_{\rm c.m.}$ for the both reactions. According to the DNS model, the use of the heavy ^{184}W isotope was more favorable to CN formation in comparison with using ^{182}W. It is explained by the fact that quasifission barrier $B_{\rm qf}$ (see Fig. 4b) for the reaction with ^{184}W is larger than one for the reaction with ^{182}W. The yield of quasifission is dominant at the subbarrier beam energies leading to capture of deformed nuclei only with the small orientation angle of its symmetry axis relative to the beam direction. This phenomenon was found by Hinde and his colleagues [19] in the ^{16}O+^{238}U reaction where they observed the increase in the anisotropy of angular distribution of the fission fragments when beam energy decreases to the subbarrier region. Its analysis has been discussed in Ref. [18] in connection with the explanation of the observed large angular anisotropy of the fission fragments. As an alternative suggestion

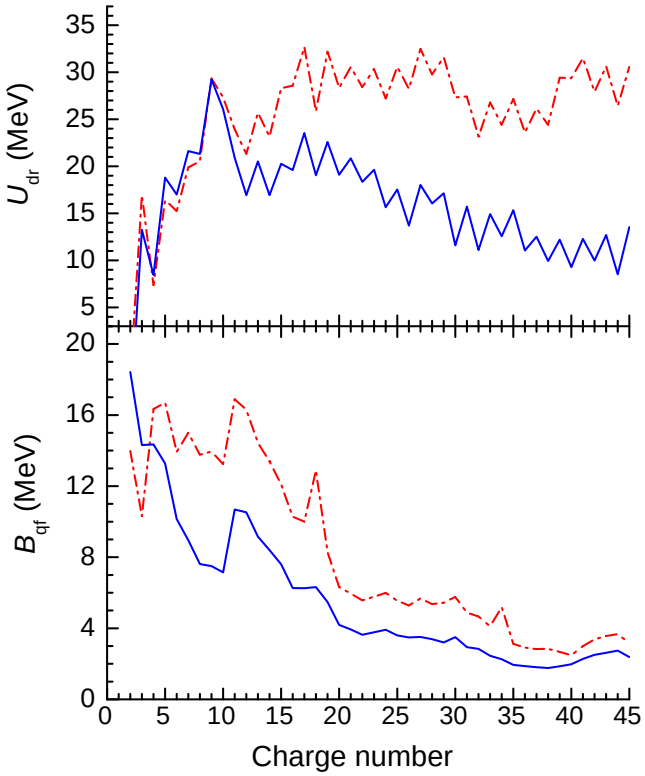

FIG. 8: (Color online) Driving potential calculated for the two different values of the orientation angles of target nucleus: $\alpha_T = 15°$ (solid line) and $\alpha_T = 45°$ (dot-dashed line) for the $^{32}S+^{184}W$ reaction.

for the origin of the observed anomaly, Liu *et al.* in Ref. [39] have put forward a new version of the preequilibrium fission model. The anomalous bump exists in the variation of the fragment anisotropy with the incident energy for the systems such as ^{19}F, ^{16}O $+^{232}Th$. Based on these studies, a new model of K pre-equilibrium fission was proposed, which can well explain the observed anomalous anisotropy. The authors of Ref. [19] analyzed in detail the angular anisotropy of fragments at low energies to show the dominant role of the quasifission in collisions of the projectile with the target nucleus when the axial symmetry axis of the latter is oriented along or near the beam direction. Large values of the anisotropy were obtained at low energies and these data were assumed to be connected with quasifission because a mononucleus or DNS formed in the near tip collisions has an elongated shape. This shape can be far from the one corresponding to the saddle point. The driving potential used in the DNS model depends on the shape of the DNS which is formed in collisions with the different orientation angles of the axial symmetry axis of deformed target. The small values of the fusion probability P_{CN} at lowest energies in the $^{32}S+^{182,184}W$ reactions are explained by the large values of B^*_{fus} for DNS formed at collisions of projectile with target

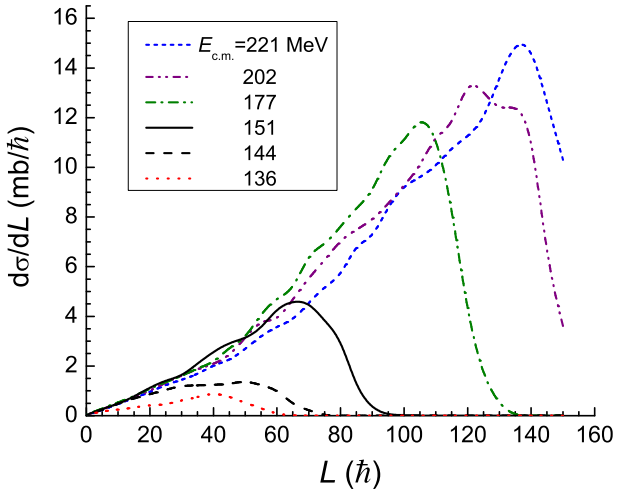

FIG. 9: (Color online) The partial quasifission excitation function calculated at different values of the collision energy $E_{\rm c.m.}$ for the ^{32}S+^{184}W reaction.

oriented close to beam direction, *i.e.* when $\alpha_{\rm T}$ is small. To demonstrate this conclusion we present in Fig. 8 the driving potential (upper panel) and quasifission barrier (lower panel) for the decay of DNS as a function of the orientation angles of the target nucleus. It is seen from the upper panel of Fig. 8 that the value of driving potential corresponding to the projectile charge number Z=16 for the small orientation angle 15° (solid line) of the target is lower than that corresponding to the larger orientation angle 45° (dashed line). The fusion probability is larger if a value of the driving potential $U_{\rm dr}(Z_{\rm proj})$ corresponding to the initial charge number of the light fragment $Z_{\rm L}$ of the DNS is at the same level with the maximum value at Z=9 along the way to complete fusion or as possible higher than this maximum value. In these cases, all nucleons of light nucleus transfer easy into heavy nucleus: $Z_{\rm L} \longrightarrow 0$ and $Z_{\rm H} \longrightarrow Z_{\rm CN}$.

The lowering of the $P_{\rm CN}$ values in Fig. 7 at collision energies $E_{\rm c.m.} > 145$ MeV is explained by decreasing the quasifission barrier $B_{\rm qf}$ as a function of the orbital angular momentum ℓ. Because the depth of the potential well being $B_{\rm qf}$ for a given charge asymmetry decreases due to the increase in the rotational energy $E_{\rm rot}$ of the DNS (for details see [10]). At the same time the intrinsic fusion barrier $B^*_{\rm fus}$ increases by increasing ℓ. At small collision energies only small values of ℓ are populated because a capture does not occur if the initial energy of projectile is not enough to overcome the Coulomb barrier of the entrance channel.

It is seen from Fig. 9 that the values $\ell > 70$ are populated at collision energies $E_{\rm c.m.} > 144$

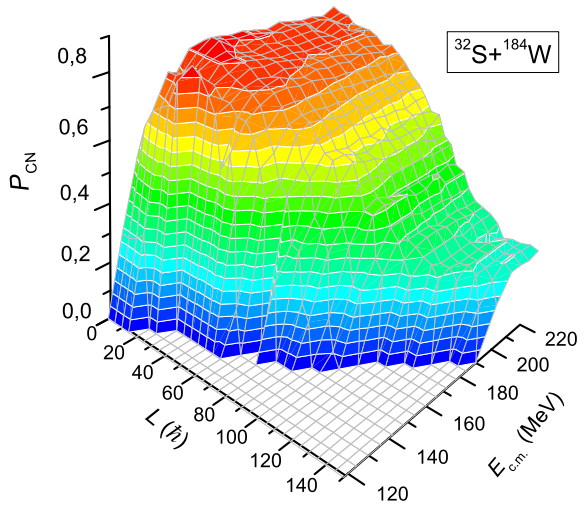

FIG. 10: (Color online) The presentation of the fusion probability $P_{\rm CN}$ for the ^{32}S+^{184}W reaction as a function of collision energy $E_{\rm c.m.}$ and initial angular momentum L.

MeV. Therefore, we conclude that the contribution of quasifission and fast fission becomes dominant at $E_{\rm c.m.} > 144$ MeV and it has an effect on the anisotropy of angular distribution which increases by increasing the collision energy. In Fig. 10, the appearance of the quasifission as a hindrance to fusion is demonstrated as a function of the collision energy and orbital angular momentum for the ^{32}S+^{184}W reaction. One can see that maximum value of $P_{\rm CN}$ (favorable condition to complete fusion) is reached at their middle values of $E_{\rm c.m.}$=135-140 MeV and at ℓ=20–25. This is connected with the fact that at these energies all orientation angles $\alpha_{\rm T}$ can contribute to the formation of compound nucleus because the Coulomb barrier for large orientation angles may be overcame. As we know, in collisions with large $\alpha_{\rm T}$ the fusion probability is large. The decrease of $P_{\rm CN}$ at larger energies is explained by the decrease in the quasifission barrier B_{qf} by increasing ℓ in collisions with all orientation angles.

In synthesis of superheavy elements by using actinide nuclei as a target the beam energy have to be larger enough than the well known Bass barrier to have possibility to include contribution of the large orientation angles. Therefore, a further increase in the beam energy leads not only to a decrease in the survival probability of the hot CN but also to the strong increasing the quasifission events. The measured anisotropy of the fragments ascribed as fission products confirmed this conclusion.

B. Anisotropy of fission fragment angular distribution and variance K_0^2 of K distribution

To clarify the role of quasifission fragments in the observed anisotropy $A_{\rm exp}$ of the fission fragment angular distribution, we calculated the anisotropies of the angular distributions of the quasifission and fusion-fission fragments. We used the approximated expression to calculate the anisotropy suggested by Halpern and Strutinski in Ref. [40] and Griffin in Ref. [41]:

$$\mathcal{A} \approx 1+\frac{\langle l^2\rangle_i \hbar^2}{4\Im_{\rm eff}{}^{(i)} T_i}, \text{ where } \frac{1}{\Im_{\rm eff}} = \frac{1}{\Im_{\|}} - \frac{1}{\Im_{\perp}}. \tag{18}$$

Here $\Im_{\rm eff}^{(i)}$ is the effective moment of inertia for the CN on the saddle point $i =$ CN or it is the effective moment of inertia for the DNS on the quasifission barrier $i =$ DNS. In the last case, we calculate $\Im_{\rm eff}$ for the DNS taking into account the possibility of different orientation angles of its constituent nuclei (see Appendix A of Ref.[18]), assuming that after capture the mutual orientations of the DNS nuclei do not change sufficiently. $\Im_{\|}$ and $\Im_{\perp}$ are the moments of inertia around the symmetry axis and a perpendicular axis, respectively.

Their values for $\Im_{\rm eff}^{\rm (CN)}$ are determined in the framework of the rotating finite range model by Sierk [33]. The temperature of CN on the saddle point is found by the expression:

$$T_{\rm CN} = \left[\frac{E_{\rm c.m.} + Q_{\rm gg} - B_{\rm f}(\ell) - E_n}{A_{\rm CN}/12}\right]^{1/2}, \tag{19}$$

where $B_{\rm f}(\ell)$ is the fission barrier height. $B_{\rm f}(\ell)$ is calculated in terms of the rotating liquid drop model by Sierk [33]. $E_{\rm n}$ is the energy carried away by the pre-saddle fission neutrons. The temperature of DNS on the quasifission barrier is determined by the expression:

$$T_{\rm DNS} = \left[\frac{(E^*_{\rm DNS} - B_{\rm qf})}{A_{\rm CN}/12}\right]^{1/2}. \tag{20}$$

An important physical quantity in the formula (18) is the variance K_0^2 of the Gaussian distribution of the K projection :

$$K_0^2 = \frac{\Im_{\rm eff} T_{\rm saddle}}{\hbar^2}. \tag{21}$$

The experimental values of K_0^2 are used to fit the angular distribution of fission fragments by formula (6) (see Ref.[23, 42]).

In Fig. 11 we compare the anisotropy measured (squares) in this work with the theoretical results for the anisotropy of the quasifission (dashed line) and fusion-fission (solid

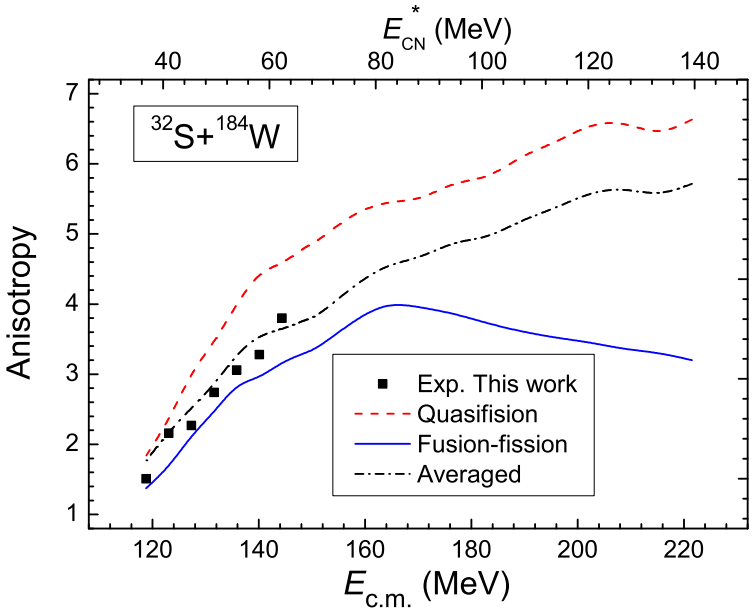

FIG. 11: (Color online) Comparison of the anisotropy measured (circles) in this work for the ^{32}S+^{184}W reaction with the theoretical results for the anisotropy of the quasifission (dashed line) and fusion-fission (solid line) fragments as function of the center-of-mass energy (bottom axis) and excitation energy of CN (top axis). The averaged values of theoretical results are presented by dot-dashed line.

line) fragments as a function of the center-of-mass energy (bottom axis) and excitation energy of the CN (top axis). The averaged theoretical anisotropy over the contributions of both mechanisms are presented by the dot-dashed line. It is seen that the averaged values of anisotropy $\mathcal{A}$ are closer to the experimental data. Consequently we confirm that the measured cross section of the fission fragment formation and their angular distribution are results of mixing of the quasifission and fusion-fission products. The dip of the solid curve corresponding to the contribution of the fusion-fission fragments is caused by the increasing the effective temperature of CN with the angular momentum $\ell < \ell_f = 70$.

In the upper panel of Fig.12, we compare experimental and theoretical values of mean square values of angular momentum. The experimental $\langle \ell^2 \rangle$ values are obtained from the measured anisotropy $\mathcal{A}_{\rm exp}$ and K_0^2 values used to fit measured angular distributions presented in Fig. 2. The theoretical values for fusion-fission and quasifission fragments are calculated by averaging ℓ^2 using the partial cross sections of the quasifission (dashed line) and complete fusion (solid line) events. The experimental data are well described with the averaged values

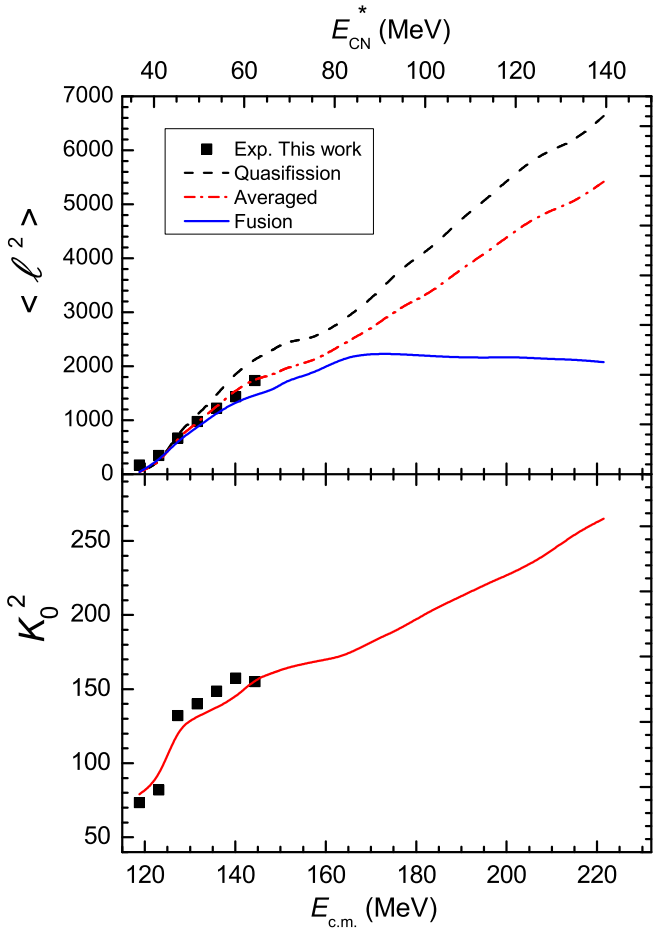

FIG. 12: (Color online) Mean square value of the angular momentum (upper panel) versus the collision energy $E_{\rm c.m.}$ for the ^{32}S+^{184}W reaction. The experimental data (solid squares) are shown in comparison with the results of DNS model which are obtained by averaging ℓ^2 by partial cross sections of the quasifission (dashed line) and complete fusion (solid line) events. In the lower panel the experimental data of this work (solid squares) for K_0^2 are compared with our theoretical results.

of ℓ^2 between the complete fusion and quasifission cross sections:

$$\langle \ell^2 \rangle = \frac{(\sigma_{\rm fus}\langle \ell^2 \rangle_{\rm fus} + \sigma_{\rm qf}\langle \ell^2 \rangle_{\rm qf})}{\sigma_{\rm fus} + \sigma_{\rm qf}}. \tag{22}$$

In the lower panel of Fig.12, the experimental data of this work (solid squares) for K_0^2 are compared with the theoretical values obtained from the description of $\mathcal{A}_{\rm exp}$ (dot-dashed line in Fig.11) and $\langle \ell^2 \rangle$ (dot-dashed line in Fig.12) extracted from the experimental data of the angular distribution of fission fragments. This comparison shows again the dominancy of the quasifission fragments into measured data.

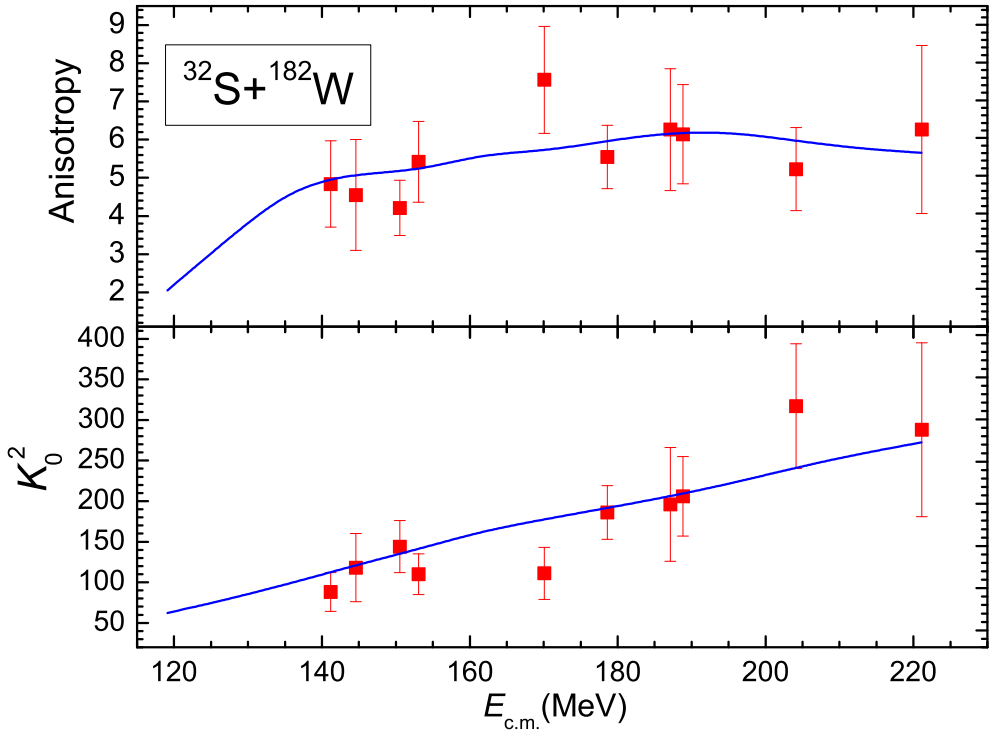

FIG. 13: (Color online) Comparison of the experimental data from Ref. [22] for K_0^2 (solid squares) and anisotropy $\mathcal{A}$ with results of the DNS model (solid line).

In Fig. 13 we compare the results of our calculation for K_0^2 with the experimental data presented in Ref. [38] for the ^{32}S+^{182}W reaction as a function of $E_{\rm c.m.}$. The good description of the experimental data of the capture excitation function for both reactions and quantities K_0^2, $\mathcal{A}_{\rm exp}$ and $< \ell^2 >$ which characterize angular distribution of the fission products by the partial capture and fusion cross sections proves the rationality of the theoretical method based on the DNS concept to analysis the fusion-fission, quasifission and fast fission mechanisms at the considered range of beam energy. We should stress that the partial fusion cross sections were used to calculate excitation function of the total evaporation residues by the advanced statistical model [11–13].

V. CONCLUSION

The fission angular distributions for the ^{32}S+^{184}W reaction have been measured at center-of-mass energies of 118.8–144.4 MeV. The experimental cross sections of fissionlike products,

the anisotropy $\mathcal{A}_{\rm exp}$, K_0^2 and $\langle \ell^2 \rangle$ values were obtained. The experimental data of this work, of Refs. [35] (capture exciation function) and [16] (excitation function of the total evaporation residues) for this reaction and the same kind of experimental data for the ^{32}S+^{182}W reaction obtained from Refs. [22, 37, 38] (capture and fusion) and [22, 38] (K_0^2 and ℓ^2) were described by the DNS model and advanced statistical model [11–13]. The measured fission excitation function was described as the capture excitation function containing quasifission and fast fission products together with fusion-fission products. The partial capture cross sections were calculated for the different orientation angles of the symmetry axis of the target nuclei ^{182}W and ^{184}W. The quadrupole (2^+) and octupole (3^-) collective excitations in ^{32}S are taken into account as amplitudes of the zero-point motion mode of surface vibration by the same way as in Ref.[27]. The total evaporation residue and fusion-fission excitation functions are calculated in the framework of the advanced statistical model using the partial fusion cross sections obtained in this work for both considered reactions. The dip of the theoretical curve from experimental data [16] for the ^{32}S+^{184}W reaction at high excitation energies $E_{\rm c.m.} > 160$ MeV is caused by the fact that statistical model can not reproduce the cross section of formation of reaction products by the nonequlibrium mechanism without formation of the compound nucleus in the statistical equlibrium state. The ER events at $E_{\rm c.m.} > 160$ seem to be connected with incomplete fusion or multinucleon transfer reactions. Because the number of evaporation residues formed from the heated and rotating CN should not increase at decreasing of the complete fusion cross section by the increase in the collision energy $E_{\rm c.m.}$. The decrease of complete fusion probability at large collision energies is connected with the increase of quasifission and fast fission. An increase in the quasifission contribution at large beam energies is connected with the angular momentum dependence of the quasifission $B_{\rm qf}$ and intrinsic fusion $B^*_{\rm fus}$ barriers: at large angular momentum of the DNS $B_{\rm qf}$ decreases and $B^*_{\rm fus}$ increases. The small quasifission barrier decreases the lifetime of DNS decreasing its possibility to be transformed into a CN [10, 17]. The fusion-fission cross section is larger than the quasifission cross section in the energy range $130 < E_{\rm c.m.} < 170$ MeV where we have $P_{\rm CN} > 0.5$ for both reactions. The contribution of the fast fission becomes comparable with the fusion-fission and quasifission products at about $E_{\rm c.m.} > 175$ MeV. The experimental data presented and analysed in this work are the smooth continuation to the lower energies of the data presented in previous published papers here cited. The theoretical descriptions of the experimental capture excitation function for both reactions

and quantities K_0^2, $< \ell^2 >$ and $\mathcal{A}_{\rm exp}$ which characterize angular distribution of the fission products were performed by the same partial capture cross sections at the considered range of beam energy. We conclude that the effects of competition between fusion and quasifission in the reaction play an important role in the dynamics process.

ACKNOWLEDGMENTS

This work was supported by the Major State Basic Research Development Program under Grant No. G2000077400 and the National Natural Science Foundation of China under Grant Nos. 10375095, 10735100, and 10811120019. A. K. Nasirov is grateful to the Istituto Nazionale di Fisica Nucleare and Department of Physics of the University of Messina and Russian Foundation for Basic Research for the support of collaboration between the Dubna and Messina groups.

---

[1] Yu. Ts. Oganessian *et al.*, Phys. Rev. C **70**, 064609 (2004).

[2] Yu. Ts. Oganessian *et al.*, Phys. Rev. C **74**, 044602 (2006).

[3] K. Morita, *et al.*, J. Phys. Soc. Japan, **73** 2593 (2004).

[4] K. Morita, *et al.*, J. Phys. Soc. Japan,**76**, 043201 (2007).

[5] B.B. Back, *et al.*, Phys. Rev. C**32**, 195 (1985)

[6] N. A. Antonenko, E. A. Cherepanov, A. K. Nasirov, V. P. Permjakov, and V. V. Volkov, Phys. Lett B **319** 425 (1993); Phys. Rev. C 51, 2635 (1995)

[7] G. Fazio, G. Giardina, A. Lamberto, R. Ruggeri, C. Saccà, R. Palamara, A. I. Muminov, A. K. Nasirov, U. T. Yakhshiev, F. Hanappe, Eur. Phys. J. A **19**, 89 (2004).

[8] G.G. Adamian, N.V. Antonenko, W. Scheid, Phys. Rev. C **68**, 034601 (2003).

[9] G. Giardina, S. Hofmann, A. I. Muminov, A. K. Nasirov, Eur. Phys. J. A **8** 205 (2000).

[10] G. Fazio, G. Giardina,. G. Mandaglio, R. Ruggeri, A. I. Muminov, A. K. Nasirov, Yu. Ts. Oganessian, A. G. Popeko, R. N. Sagaidak, A. V. Yeremin, S. Hofmann, F. Hanappe, C. Stodel, Phys.Rev. C **72** 064614 (2005).

[11] A. D' Arrigo, G. Giardina, M. Herman, and A. Taccone, Phys. Rev. C **46**, 1437 (1992).

[12] A. D' Arrigo, G. Giardina, M. Herman, A. V. Ignatyuk, A. Taccone, J. Phys. G **20**, 365 (1994).

[13] R. N. Sagaidak, V. I. Chepigin, A. P. Kabachenko, J. Rohac, Yu. Ts. Oganessian, A. G.

Popeko, A. A. Yeremin, A. D'Arrigo , G. Fazio, G. Giardina, M. Herman, R. Ruggeri, and R. Stiricle, J. Phys. G **24**, 611 (1998).

[14] A. Sobiczewski, M. Kowal, Int. Jour. of Mod. Phys. E **18**, No: 4, 869 (2009)

[15] I. Muntian, Z. Patyk, A. Sobiczewski, Phys. of At. Nuclei **66** Issue: 6, 1015 (2003).

[16] B. B. Back, D. J. Blumenthal, C. N. Davids, D. J. Henderson, R. Hermann, D. J. Hofman, C. L. Jiang, H. T. Penttilä, and A. H. Wuosmaa, Phys. Rev. C **60**, 044602 (1999).

[17] Avazbek Nasirov, Akira Fukushima, Yuka Toyoshima, Yoshihiro Aritomo, Akhtam Muminov, Shuhrat Kalandarov, Ravshanbek Utamuratov, Nucl. Phys. A **759**, 342 (2005).

[18] A.K. Nasirov, A.I. Muminov, R.K. Utamuratov, G. Fazio, G. Giardina, F. Hanappe, G. Mandaglio, M. Manganaro, and W. Scheid, Eur. Phys. J. A **34**, 325 (2007).

[19] D.J. Hinde, M. Dasgupta, J.R. Leigh, J.C.Mein, C.R.Morton, J.O. Newton, H. Timmers, Phys. Rev. C **53**, 1290 (1996).

[20] M. G. Itkis et al., Nucl. Phys. A**734**, 134 (2004).

[21] G. N. Knyazheva, E. M. Kozulin, R. N. Sagaidak, A. Yu. Chizhov, M. G. Itkis, N. A. Kondratiev, V. M. Voskressensky, M. Stefanini, B. R. Behera, L. Corradi, Phys. Rev. C **75**, 064602 (2007).

[22] J.G. Keller, B.B. Back, B.G. Glagola, D. Henderson, S.B. Kaufman, S.J. Sanders, R.H. Siemssen, F. Videback, B.D. Wilkins, and A. Worsham, Phys.Rev.C **36**, 1364 (1987).

[23] J. R. Huizenga, A. N. Behkami, and L. G. Moretto, Phys. Rev. **177** 1826 (1969)

[24] C. Gregoire, C. Ngo, E. Tomasi, B. Remaud, F. Scheuter, Nucl.Phys. **A387**, 37c (1982).

[25] V. E. Viola, K. Kwiatkowski, and M. Walker, Phys. Rev. C **31** 1550 (1985)

[26] A. K. Nasirov, G. Giardina, G. Mandaglio, and M. Manganaro, F. Hanappe, S. Heinz and S. Hofmann, A. I. Muminov, W. Scheid Phys.Rev. C **79**, 024606 (2009).

[27] G. Fazio, G. Giardina, F. Hanappe, G. Mandaglio, M. Manganaro, A. I. Muminov, A. K. Nasirov, and C. Sacca, J. Phys. Soc. Jpn. **77**, 124201 (2008).

[28] V.V. Volkov, in Contributed Papers of Nucleus-Nucleus Collision II, Visby, 1985, edited by B. Jakobson and K. Aleclett (North-Holland, Amsterdam, 1985), Vol.1, p.54; Izv. Akad. Nauk SSSR Ser. Fiz. 50, 1879 (1986); in Proceedings of International School-Seminar on Heavy Ion Physics, Dubna, 1986, D7-87-68 (Dubna, 1987), p. 528; in Proceedings of the 6th International Conference on Nuclear Reaction Mechanisms, Varenna, 1991, edited by E. Gadioli (Ricerca Scientifica ed Educasione Permanente Supplemento n.84, 1991), p.39. on Heavy Ion Physics

[29] P. Moller and J. R. Nix, Atomic Data and Nuclear Data **39**, 213 (1988).

[30] S. Raman, C. H. Malarkey, W. T. Milner, C. W. Nestor, Jr., and P. H. Stelson, Atomic Data and Nuclear Data **36**, 1 (1987).

[31] R. H. Spear, Atomic Data and Nuclear Data **42**, No. 1, 55 (1989).

[32] G. Fazio, G. Giardina, G. Mandaglio, F. Hanappe, A. I. Muminov, A. K. Nasirov, W. Scheid, L. Stittge, Mod. Phys. Lett. A Vol. **20**, No. 6, 391 (2005).

[33] A. J. Sierk, Phys. Rev. C **33**, 2039 (1988).

[34] G. Fazio, G. Giardina, A. Lamberto, A. I. Muminov, A. K. Nasirov, F. Hanappe and L. Stuttge, Eur. Phys. Jour. A **22** 75 (2004).

[35] D. J. Hofmann, B. B. Back, and P. Paul, Phys. Rev. C**51**, 2597 (1995).

[36] K. Pomorski, B. Nerlo-Pomorska, A. Surowiec, M.Kowal, J. Bartel, K. Dietrich, J. Richert, C. Schmitt, B. Benoit, E. de Goes Brennand, L. Donadille, C. Badimong, Nucl. Phys. A **679** 25 (2000).

[37] S. Mitsuoka, H. Ikezoe, K. Nishio, and J. Lu, Phys. Rev. C**62**, 054603 (2000).

[38] B. B. Back, P. B. Fernandez, B. G. Glagola, D. Henderson, S. Kaufman, J. G. Keller, S. J. Sanders, F. Videbk, T. F. Wang, and B. D. Wilkins, Phys. Rev. C**53**, 1734 (1996).

[39] Z. H. Liu, H.Q. Zhang, J.C. Xu, Y. Qiao, X. Qian, and C.J. Lin, Phys. Lett. B **353**, 173 (1995).

[40] I. Halpern and V. M. Strutinski, Proceeding of the Second United National International Conference on the Peaceful Uses of Atomic Energy, Geneva, 1958 (United Nations, Geneva, 1958), Vol. 15, p.408.

[41] J. J. Griffin, Phys. Rev **116**, 107 (1959).

[42] D.J. Hinde, A. C. Berriman, M. Dasgupta, J. R. Leigh, J. C. Mein, C. R. Morton, and J. O. Newton, Phys. Rev. C**60**, 054602 (1999).